Water Level in Observation Wells Simulated From Fracture and Matrix Water Heads Outputted by Dual-Continuum Hydrogeological Models: POWeR-FADS

B. Jeannot, L. Schaper, F. Habets

AGU ADVANCING EARTH AND SPACE SCIENCES

Water Resources Research

RESEARCH ARTICLE
10.1029/2023WR034652

Special Section:
Quantifying human interferences in hydrologic process modeling

Water Level in Observation Wells Simulated From Fracture and Matrix Water Heads Outputted by Dual-Continuum Hydrogeological Models: POWeR-FADS

B. Jeannot[1,2], L. Schaper[1], and F. Habets[2]

[1]Commissariat à l'Énergie Atomique et aux Énergies Alternatives, Direction des Applications Militaires, Direction Île-de-France, Arpajon, France, [2]CNRS UMR 8538, Laboratoire de Géologie, École Normale Supérieure, PSL Research University, Paris, France

Abstract Do observation wells in fractured porous aquifers measure water head in the fracture network, water head in the matrix, or some combination of both? This question necessarily arises when calibrating dual-continuum hydrogeological models against on-field data. One can assume that observation wells measure fracture water head, because matrix permeability is negligible compared to fracture permeability. Nevertheless, this reasoning is invalid for wells poorly-connected to the fractures. Yet, the possibility of such a poor connection at given depths has never been implemented in a physics-based manner when comparing matrix and fracture water heads simulated by dual-continuum models to on-field data. To fill this knowledge gap, a physically based, easy to calibrate, open-source postprocessing tool, POWeR-FADS (Program for Observation Well Representation in Fractured Aquifer Dual-continuum Simulations), available at https://github.com/BJeannot1/POWeR-FADS, has been developed. It introduces as parameters well geometry and the altitude of lowest interception of the fractures by the well. From these, POWeR-FADS nonintrusively postprocesses time series of matrix and fracture water heads at the well, as simulated by any planar, bidimensional dual-continuum hydrogeological model, to calculate water exchanges involving the observation well and thus the evolution of water level in the well. Synthetic test cases show that POWeR-FADS makes it possible to simulate peculiar behaviors that are similar to patterns actually observed by the authors in on-site observation wells of a fractured porous aquifer, like "floors" in observed water levels, delayed but sharp rises at the beginning of recharge events, or inflexion points accelerating the drawdown velocity during the recession phase.

Key Points:

- A program is made to simulate the water level in observation wells from matrix and fracture water heads computed by dual-continuum models
- For wells poorly connected to the fractures, the code simulates patterns that could not be modeled by a dual-continuum model alone
- This postprocessing tool is easy to use, as its most sensitive parameter can be deduced from drill cores or observation well data

Correspondence to:
B. Jeannot,
bjeannot.pro@gmail.com

Citation:
Jeannot, B., Schaper, L., & Habets, F. (2023). Water level in observation wells simulated from fracture and matrix water heads outputted by dual-continuum hydrogeological models: POWeR-FADS. *Water Resources Research*, *59*, e2023WR034652. https://doi.org/10.1029/2023WR034652

Received 13 FEB 2023
Accepted 5 JUL 2023

Author Contributions:
Conceptualization: B. Jeannot, L. Schaper, F. Habets
Data curation: B. Jeannot, L. Schaper
Formal analysis: B. Jeannot
Funding acquisition: L. Schaper, F. Habets
Methodology: B. Jeannot, L. Schaper, F. Habets
Project Administration: L. Schaper, F. Habets
Software: B. Jeannot
Supervision: L. Schaper, F. Habets
Validation: B. Jeannot, L. Schaper, F. Habets
Visualization: B. Jeannot
Writing – original draft: B. Jeannot
Writing – review & editing: B. Jeannot, L. Schaper, F. Habets

1. Introduction

The main issue when modeling the hydrogeology of fractured porous rocks is that water simultaneously flows slowly through the soil matrix, but relatively quickly through preferential pathways in a network of fractures. A wide range of modeling approaches have been developed to deal with the complexity of these systems. Berkowitz (2002), Neuman (2005), and more recently Berre et al. (2019) provide overviews of the state of the art in this domain.

Fractures can be modeled by explicitly defining their geometry (e.g., Flemisch et al., 2018; Hyman et al., 2022; Sandve et al., 2012). This is appropriate for individual fractures or conduits that have a dominating, structural impact on flow processes (Berre et al., 2019). Otherwise, the fracture network can be considered implicitly by an equivalent continuum. In this case, if exchanges between the matrix and the fractures are fast in comparison to flow in the rock system, the two media can be assumed to be at equilibrium, so that one can model the whole system as a single equivalent continuum (e.g., Hu & Walsh, 2021; Liu et al., 2000; MousaviMirkalaei et al., 2022; Peters & Klavetter, 1988; Saevik et al., 2014). In the absence of such an equilibrium, a common practice consists in modeling the system by considering the matrix and the fractures as two distinct continua, each of them with its own hydrodynamic parameters, and linked to the other by an exchange term. This dual-continuum concept was first introduced by Barenblatt et al. (1960) and Warren and Root (1963), and has since then been implemented by many authors (e.g., Al-Shaalan et al., 2003; Choi et al., 1997; Gerke & van Genuchten, 1993a; Robineau et al., 2018; Rüdiger et al., 2022). Dual-continuum approaches differ according to their level of complexity, with a distinction between dual-porosity models and dual-porosity/dual-permeability models, also simply called dual-permeability models (e.g., Berkowitz, 2002; Neuman, 2005). The difference is that dual-porosity models neglect flow in the matrix because of generally low conductivities compared to the fracture medium, while dual-permeability models do not make this assumption.

As the matrix and fracture continua are not at equilibrium in dual-continuum models, this kind of approach simulates fields of water head for each of the two media. This can become a problem when trying to calibrate the parameters of a dual-continuum model using data from observation wells: should the water levels seen in the observation wells be compared to the simulated water heads in the matrix, to those in the fracture, or to a function involving both?

Studies involving the calibration of the hydrodynamic parameters of a dual-continuum model over a real or synthetic test case generally compare the water levels in the wells to the simulated water head in the fracture continuum (e.g., Delay et al., 2017; Kaczmaryk & Delay, 2007a, 2007b; Robineau et al., 2018). The reasoning is that, as hydraulic conductivities in the fracture medium are generally several orders of magnitude higher than those in the matrix, the water level in the well can be assumed to be mainly controlled by the total water head in the fracture medium.

However, such a hypothesis is invalid in the case of a poor connection between the fractures and the well. For instance, Jazayeri et al. (2011) observed from an analysis of on-field data that the connectivity of observation wells with the high-permeability flow path has a determining impact on water levels measured in the wells; in particular, the wells that are the least connected to the fracture network and karstic conduits exhibit more inertial responses, as they are more influenced by the matrix. Bogdanov et al. (2003) reached the same conclusion when modeling a synthetic fractured aquifer with an approach involving an explicit representation of fractures.

This case of a poor connection of the well with the fractures is particularly likely to happen in aquifers where fractures are mainly oriented subvertically, where fracture density is locally low, or for wells with a low radius. In an attempt to deal with this situation when using a dual-continuum approach, Ackerer et al. (2014) considered, for a calibration of such a model on a synthetic test case, that the water level in the well is a linear combination of water heads in the matrix and in the fracture.

Incidentally, such a mixing of water from the matrix and from the fractures at the well is known to produce complex flow phenomena. For example, several studies have suggested that a non-negligible contribution of the matrix to flow to the well could generate a lack of reciprocity in interference testing of karstic aquifers (Delay et al., 2011; Sanchez-Villa et al., 2016). In short, reciprocity is a principle initially introduced by Lorentz (1896) that is generally valid for diffusion equations, which states that a stress at location B generates a response at location A equivalent to the response in B for the same stress in A.

In spite of such a complexity of flow processes at the well, to the authors' knowledge, and similarly to the observation made by Wang et al. (2020), only very few studies have tried to extend the simulations of a dual-continuum model to calculate the water level in the well by taking into account its geometry in a physically-based manner. Dougherty and Babu (1984) explicitly described the geometry of the well to simulate, in a dual-continuum fashion, radial flow to a pumping well. They assumed, however, that only the fracture medium exchanges water with the well. More recently, Wang et al. (2020) went further by including direct exchanges between the pumping well and the matrix in their simulation. Nevertheless, both studies were specifically oriented toward radial flow at a pumping well in a confined aquifer, and not toward observation wells in normal flow conditions in confined or unconfined aquifers. In addition, and more importantly, there is a need in dual-continuum models to physically represent the possibility of a poor connection between the well and the fractures at given depths, as this would justify that exchanges between the matrix and the well are indeed non-negligible in comparison to exchanges between the fractures and the well.

The present study intends to fill this knowledge gap by describing, testing, and discussing a Program for Observation Well Representation in Fractured Aquifer Dual-continuum Simulations (POWeR-FADS). This model postprocesses time series of water head at an observation well respectively in the fracture and matrix media, as simulated by any planar, bidimensional dual-continuum hydrogeological model, to simulate the water level in the well over time. POWeR-FADS performs its calculations in a physically based way, by calculating exchange fluxes between the well and each of the two media as a function of head gradients, and introduces as a parameter the altitude of lowest interception of the fracture network by the well. This is a low-parameterized way of describing in the simulations the level of connection between the well and the fractures. The tool, archived in Jeannot et al. (2022a) and available in its latest release at https://github.com/BJeannot1/POWeR-FADS, helps to improve the interpretation of data from observation wells of fractured porous aquifers when using bidimensional dual-media hydrogeological models.

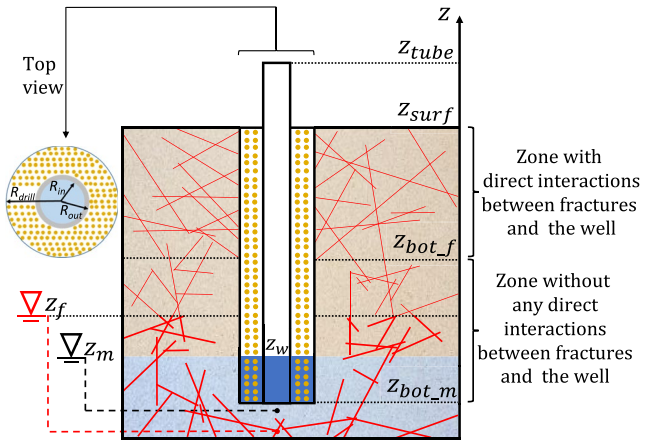

Figure 1. Physical model used in POWeR-FADS for an observation well in a fractured aquifer. R_{in}, R_{out}, and R_{drill} are respectively the inner, outer, and drill radii of the observation well. The yellow dots represent the soil of porosity ω_{drill} used to fill the space between R_{out} and R_{drill}. z_{tube} and z_{surf} are respectively the altitude of the top of the well and of the surface. The plain red lines represent the fracture network. Among them, the bold lines represent the saturated portion of the fracture network. The brown and blue backgrounds represent respectively the saturated and unsaturated zones of the matrix. z_m and z_f are the water heads respectively in the matrix and in the fracture network, and z_w is the water level in the well. z_{bot_m} and z_{bot_f} are respectively the altitude of the bottom of the well and the altitude of the lowest interception of the well by the fracture network. The absence of any direct water exchanges between the fracture network and the well below z_{bot_f} has a significant impact on z_w. For example, for the represented situation where both z_m and z_f are below z_{bot_f}, and assuming z_m and z_f to be constant over time, then at steady state z_w is equal to z_m.

A concise outline of this paper is as follows. In Section 2, the physical and numerical models underpinning POWeR-FADS are detailed. Section 3 presents synthetic test cases exhibiting the ability of the developed model to simulate peculiar flow patterns. Section 4 discusses the limitations, parameterization, and applications of the model. Finally, Section 5 presents the conclusions of this research.

2. Description of the Developed Model: POWeR-FADS

2.1. Physical Model

We consider a fractured aquifer, either confined or unconfined, that is monitored by an observation well. The total water head (which is the sum of the altitude and of the pressure head) in the matrix and in the fracture network over time in the vicinity of the well, respectively denoted by z_m [L] and z_f [L], are assumed to be calculated beforehand by a planar, bidimensional dual-continuum hydrogeological model, which did not explicitly take into account the geometry of the well in the simulations.

The presence of the well is assumed to have a negligible effect on the time series of z_m and z_f, so that fluxes between either of the two media and the well only affect the water level in the observation well, denoted by z_w [L]. This enables POWeR-FADS to be built as a nonintrusive tool that postprocesses the results of the dual-continuum model. Moreover, POWeR-FADS assumes an instantaneous hydrostatic equilibrium along the vertical direction z for both z_m and z_f, so that they are constant along z. Because of this assumption, POWeR-FADS does not require as input a full vertical profile of water heads in the matrix and in the fractures at the well, but only a value that is constant along z. This makes it compatible for use in the postprocessing of bidimensional models. An instantaneous hydrostatic equilibrium is also assumed in the well below z_w, so that the total water head in the well below altitude z_w is equal to z_w. Above altitude z_w, the well is assumed to be at atmospheric pressure, so that the total water head is equal to the altitude. The implications of all these assumptions are discussed more thoroughly in Section 4.1.

For characterizing the well on a horizontal cross-section, POWeR-FADS needs as parameters the inner radius and outer radius of its tube, denoted respectively by R_{in} [L] and R_{out} [L], the drill radius R_{drill} [L] that was used to drill a hole in the ground to set up the well, and the porosity of the material used to fill the space between R_{out} and R_{drill}, denoted by ω_{drill} [-]. z_w is assumed to be uniform from the center of the well to R_{drill}.

For describing the well on a vertical cross-section, POWeR-FADS requires as parameters the altitude of the top of the tube z_{tube} [L], the altitude of the surface z_{surf} [L], and the altitude of the bottom of the well z_{bot_m} [L]. It assumes that the tube is regularly perforated and therefore does not slow down flow from and out of the observation well. On top of these initial considerations, POWeR-FADS introduces as a parameter the altitude of the lowest interception of the fracture network by the well, denoted by z_{bot_f} [L]. Between z_{bot_f} and z_{surf} , the well is assumed to intercept the fracture network continuously. On the contrary, below z_{bot_f}, the fracture network cannot exchange any water directly with the well. In comparison, the matrix medium can potentially exchange water with the well from z_{bot_m} to z_{surf}. These elements are represented in Figure 1.

2.2. Governing Equations of the Numerical Model

POWeR-FADS simulates the evolution over time of the water level in the well, z_w, by means of the following governing equation:

$$\frac{\partial z_w}{\partial t} = -V(z_w, z_m, z_f) \quad (1)$$

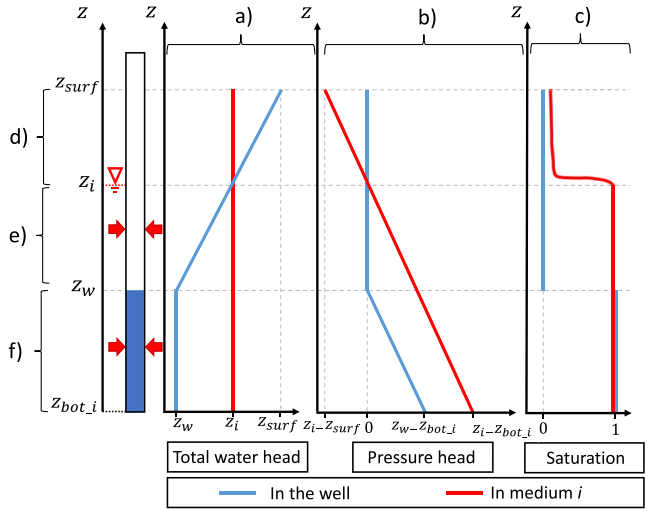

Figure 2. Total water head (a), pressure head (b), and water saturation (c) assumed by POWeR-FADS as a function of altitude z, both in the well and in medium i, in the case where the water level in the well, z_w, is below or equal to the total water head in medium i, denoted by z_i. (d) Above z_i, (e) between z_i and z_w, and (f) below z_w. z_{bot_i} represents either the altitude of the bottom of the well (if medium i is the matrix) or the altitude of lowest interception of the fracture network by the well (if medium i is the fracture network). z_{surf} is the altitude of the surface. Red arrows show in what part of the well water infiltrates from medium i. The schematic representation of saturation in medium i along z represents the general shape of this curve as calculated by the van Genuchten equation (van Genuchten, 1980). In the figure, it has been assumed that z_i and z_w are between z_{bot_i} and z_{surf}. Cases where z_i and/or z_w are either above z_{surf} or below z_{bot_i} are a trivial variation of this example.

In Equation 1, t [T] is the time and V [L.T^{-1}] is the drawdown velocity. A positive V stands for a decreasing z_w, and a negative V stands for an increasing z_w. V can be decomposed as follows:

$$V(z_w, z_m, z_f) = V_m(z_w, z_m) + V_f(z_w, z_f) \quad (2)$$

Where V_m and V_f [L.T^{-1}] are the parts of V that depend respectively on the well-matrix and well-fractures exchange fluxes.

Considering that the index i is either equal to m or f, referring either to the matrix or to the fracture network, $V_i(z_w, z_i)$ [L.T^{-1}] is calculated by dividing the flux, denoted by $Q_i(z_w, z_i)$ [L^3.T^{-1}], from the well to the medium i, by an equivalent area S_{eq} [L^2]. S_{eq} aims at representing both the interior of the tube of the well, which is characterized by a porosity of 1, and the area between R_{out} and R_{drill}, which is filled by a material of porosity ω_{drill}. This yields Equation 3:

$$V_i(z_w, z_i) = \frac{Q_i(z_w, z_i)}{S_{eq}} \text{ ; where } S_{eq} = \pi {R_{in}}^2 + \pi \omega_{drill} \left[{R_{drill}}^2 - {R_{out}}^2 \right] \quad (3)$$

$Q_i(z_w, z_i)$ is obtained by integrating the flux per unit of surface from the well to the medium i, denoted by q_i [L.T^{-1}], over the surface of the well that is in contact with the considered medium. Along the vertical direction, for the matrix, this contact surface ranges from altitude z_{bot_m} to altitude z_{surf}. For the fracture, and as represented in Figure 1, it ranges from altitude z_{bot_f} to z_{surf}. As a reminder, this prevents all flow between the fracture and the well below z_{bot_f}. It is also worth noting that the upper limit of the contact surface is z_{surf}, even for confined aquifers. Along the horizontal direction, provided the well is not at the exact location of a flow singularity, it can be assumed that at a given altitude z, q_i is uniform around the well. As a result, $Q_i(z_w, z_i)$ can be expressed as follows:

$$Q_i(z_w, z_i) = 2\pi R_{drill} \int_{z_{bot\_i}}^{z_{surf}} q_i(z_w, z_i, z) dz \quad (4)$$

Before going further, one needs to determine the expression of the total water head in the well, denoted by H_w [L], as a function of z. As stated before, a hypothesis of instantaneous hydrostatic equilibrium along z is made below z_w, so that $\frac{\partial H_w}{\partial z} = 0$ in that domain. Above z_w, the well is assumed to be filled only with atmospheric air; therefore, the pressure head profile in this part, expressed relative to atmospheric pressure, is assumed to be constant and equal to zero. This results in:

$$H_w(z) = \begin{matrix} z_w \text{ if } z \leq z_w \\ z \text{ if } z > z_w \end{matrix} \quad (5)$$

Similarly, because of the hypothesis of instantaneous hydrostatic equilibrium along z in the media, the total water head z_i in medium i is independent of z.

Under the above hypotheses, as shown in Figures 2cd and 3cd, in the domain where $z \geq z_i$, $z \geq z_w$, and $z \leq z_{surf}$, saturation is null in the well and positive in medium i. Yet water cannot flow from the unsaturated zone of medium i to the well, because the total water head in the well is greater than the total water head in medium i, as shown in Figures 2ad and 3ad. As a consequence, the range of the integral in Equation 4 can be narrowed:

$$Q_i(z_w, z_i) = 2\pi R_{drill} \int_{z_{bot\_i}}^{\max(z_{bot\_i}, \min(z_{surf}, \max(z_i, z_w)))} q_i(z_w, z_i, z) dz \quad (6)$$

For any z such that $z_{bot_i} \leq z \leq \max(z_{bot\_i}, \min(z_{surf}, \max(z_i, z_w)))$, q_i is calculated as a first-order exchange term, depending on the total water head difference between the well and the medium i and on the hydraulic conductivity at the interface between the well and the medium, denoted by $\overline{K_i}$ [L.T^{-1}]:

$$q_i(z_w, z_i, z) = \overline{K_i} \frac{H_w(z) - z_i}{\Delta e} \quad (7)$$

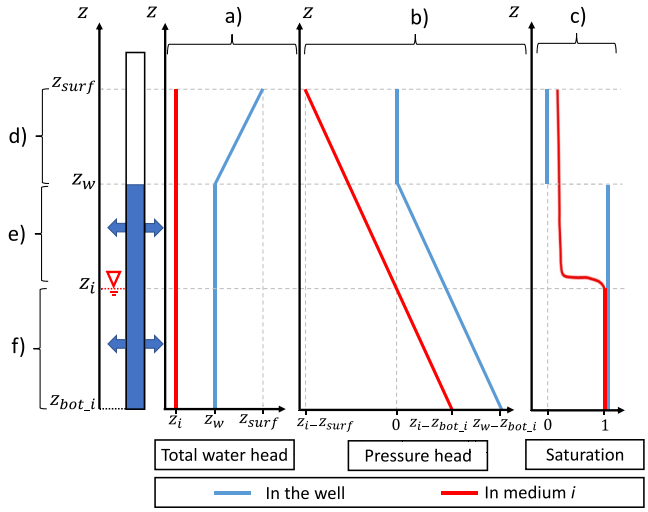

Figure 3. Total water head (a), pressure head (b), and water saturation (c) assumed by POWeR-FADS as a function of altitude z, both in the well and in medium i, in the case where the water level in the well, z_w, is above the total water head in medium i, denoted by z_i. (d) Above z_w, (e) between z_i and z_w, and (f) below z_i. z_{bot_i} represents either the altitude of the bottom of the well (if medium i is the matrix) or the altitude of lowest interception of the fracture network by the well (if medium i is the fracture network). z_{surf} is the altitude of the surface. Blue arrows show in what part of the well water exfiltrates to medium i. The schematic representation of saturation in medium i along z represents the general shape of this curve as calculated by the van Genuchten equation (van Genuchten, 1980). In the figure, it has been assumed that z_i and z_w are between z_{bot_i} and z_{surf}. Cases where z_i and/or z_w are either above z_{surf} or below z_{bot_i} are a trivial variation of this example.

In Equation 7, if the saturation in medium i at altitude z is equal to 1 (as depicted in Figures 2cf, 2ce, and 3cf), then $\overline{K}_i$ is equal to the saturated hydraulic conductivity of medium i, denoted by Ks_i [L.T^{-1}]. Conversely, if saturation in medium i at altitude z is below 1 (as depicted in Figure 3ce), then Figure 3 shows that saturation in the well is necessarily equal to 1. Therefore, in this case, $\overline{K}_i$ is set to be equal to the mean of Ks_i and of the hydraulic conductivity at altitude z in medium i, denoted by K_i [L.T^{-1}], which is calculated by the Mualem-van Genuchten formula (Mualem, 1976; van Genuchten, 1980) using as input a pressure derived from the assumption of a hydrostatic profile pressure. The mean can be either the arithmetic or geometric mean, both options being possible in POWeR-FADS. This expression of $\overline{K}_i$ makes it possible to take into account to some extent that water flowing from the well locally increases the saturation level in the medium i, and thus the hydraulic conductivity at the interface. Δe [L] is a coupling length (i.e., an empirical thickness of the interface between the well and the media).

Finally, injecting Equations 7, 6, and 3 in Equation 2 yields the full expression of V:

$$V(z_w, z_m, z_f) = \frac{2R_{\text{drill}}}{\Delta e\left[{R_{\text{in}}}^2 + \omega_{\text{drill}}\left({R_{\text{drill}}}^2 - {R_{\text{out}}}^2\right)\right]} \sum_{i=m,f} \int_{z_{\text{bot\_}i}}^{\max\left(z_{\text{bot\_}i}, \min\left(z_{\text{surf}}, \max\left(z_i, z_w\right)\right)\right)} \overline{K}_i \left[H_w(z) - z_i\right] dz \tag{8}$$

2.3. Implicit Discretization in Time and Resolution

Equation 1 does not have a general analytical solution and can be highly nonlinear, in particular because it involves the Mualem-van Genuchten formula through Equation 8. Consequently, it is solved numerically. First, the integral in Equation 8 is calculated by rectangular integration. In addition, in order to prevent numerical oscillations and to be able to calculate z_w with time steps potentially as large as those at which z_m and z_f are available, POWeR-FADS discretizes the equation implicitly in time. This means using the value of the state variable z_w at the next time in order to calculate V. Also, z_m and z_f are evaluated halfway through times n and $n+1$, assuming a linear evolution between these times. Equation 1 then becomes:

$$z_w^{n+1} - z_w^n = -V\left(z_w^{n+1}, \frac{z_m^n + z_m^{n+1}}{2}, \frac{z_f^n + z_f^{n+1}}{2}\right) * \Delta t \tag{9}$$

In Equation 9, exponents n and $n+1$ are used to respectively represent variables at times n and $n+1$, and Δt [T] is the time step between these times. In order to initialize the problem, z_w^0 can either be user-defined or set automatically by POWeR-FADS from values of z_m^0 and z_f^0, with the following equation:

$$\begin{cases} z_w^0 = \min\left(z_f^0, z_{\text{tube}}\right) \text{if } z_f^0 \geq z_{\text{bot\_}f} \\ z_w^0 = \min\left(z_m^0, z_{\text{bot\_}f}\right) \text{ if } z_f^0 < z_{\text{bot\_}f} \end{cases} \tag{10}$$

Equation 10 results from the assumptions that a steady state has been reached and that $Ks_f \gg Ks_m$.

The value of z_w^{n+1} is then found by solving Equation 9 iteratively, using a Gauss-Newton scheme, as detailed below. $z_w^{n+1,k}$ [L] designates the approximation of z_w^{n+1} at the iteration of convergence k. For $k = 0$, as a first guess, the chosen approximation of z_w^{n+1} is $z_w^{n+1,0} = z_w^n$, although this is a satisfactory approximation only when flow is reaching steady state.

The residual quantity at iteration k, denoted by F^k [L], is then defined as follows:

$$F^k = z_w^{n+1,k} - z_w^n + V\left(z_w^{n+1,k}, \frac{z_m^n + z_m^{n+1}}{2}, \frac{z_f^n + z_f^{n+1}}{2}\right) * \Delta t \tag{11}$$

If $z_w^{n+1,k} = z_w^{n+1}$, then injecting Equation 9 into Equation 11 gives $F^k = 0$. Therefore, if $z_w^{n+1,k}$ is a satisfactory approximation of z_w^{n+1}, then $F^k \approx 0$. In practice this is tested by checking if $|F^k| < \varepsilon$, where ε [L] is a convergence criterion to be set to a near-zero positive value. If, on the contrary, calculations yield $|F^k| \geq \varepsilon$, then $z_w^{n+1,k}$ is not a satisfactory approximation of z_w^{n+1}. As a result, a new approximation of z_w^{n+1}, denoted by $z_w^{n+1,k+1}$, must be found.

In order to do so, a development of F^{k+1} relative to $z_w^{n+1,k}$ is made, neglecting all terms of order greater than 1:

$$F^{k+1} \approx F^k + \frac{\partial F^k}{\partial z_w^{n+1,k}} \Delta^k \tag{12}$$

With:

$$\Delta^k = z_w^{n+1,k+1} - z_w^{n+1,k} \tag{13}$$

In Equation 12, $\frac{\partial F^k}{\partial z_w^{n+1,k}}$ is calculated by deriving Equation 11:

$$\frac{\partial F^k}{\partial z_w^{n+1,k}} = 1 + \frac{\partial V\left(z_w^{n+1,k}, \frac{z_m^n + z_m^{n+1}}{2}, \frac{z_f^n + z_f^{n+1}}{2}\right)}{\partial z_w^{n+1,k}} * \Delta t \tag{14}$$

In Equation 14, $\frac{\partial V\left(z_w^{n+1}, \frac{z_m^n + z_m^{n+1}}{2}, \frac{z_f^n + z_f^{n+1}}{2}\right)}{\partial z_w^{n+1,k}}$ is calculated by deriving the expression of V from Equation 8.

If $z_w^{n+1,k+1}$ is a satisfactory approximation of z_w^{n+1}, then $F^{k+1} \approx 0$. As a consequence, provided that $\frac{\partial F^k}{\partial z_w^{n+1,k}} \neq 0$, Equation 12 yields:

$$\Delta^k \approx \frac{-F^k}{\frac{\partial F^k}{\partial z_w^{n+1,k}}} \tag{15}$$

Injecting Equation 15 into Equation 13 leads to a value of $z_w^{n+1,k+1}$:

$$z_w^{n+1,k+1} = z_w^{n+1,k} - \frac{F^k}{\frac{\partial F^k}{\partial z_w^{n+1,k}}} \tag{16}$$

So as to facilitate convergence, Equation 16 is modified to introduce a randomized relaxation coefficient λ^k [-]. Compared to Equation 16, this reduces the absolute difference between $z_w^{n+1,k+1}$ and $z_w^{n+1,k}$, which helps to prevent divergence at the cost of a slower convergence toward a suitable approximation of z_w^{n+1}:

$$z_w^{n+1,k+1} = z_w^{n+1,k} - \lambda^k \frac{F^k}{\frac{\partial F^k}{\partial z_w^{n+1,k}}} \text{where } 0.1 < \lambda^k < 1 \tag{17}$$

The validity of this new approximation of z_w^{n+1} must then be tested. This is done by repeating the above process from Equation 11, while incrementing the value of k by 1. Such iterations continue until an approximation of z_w^{n+1} meets the convergence criterion.

Once a correct approximation of z_w^{n+1} has been calculated through the procedure described above, a posterior correction is applied in order to make sure that the calculated value has a physical meaning. POWeR-FADS caps z_w^{n+1} at the bottom end of the well by $z_{\text{bot\_}m}$, as the water level in the well cannot be lower than the bottom of the well, and at the higher end of the well by z_{tube}, to represent the possibility of water overflowing from the top of the tube in the case of a confined aquifer.

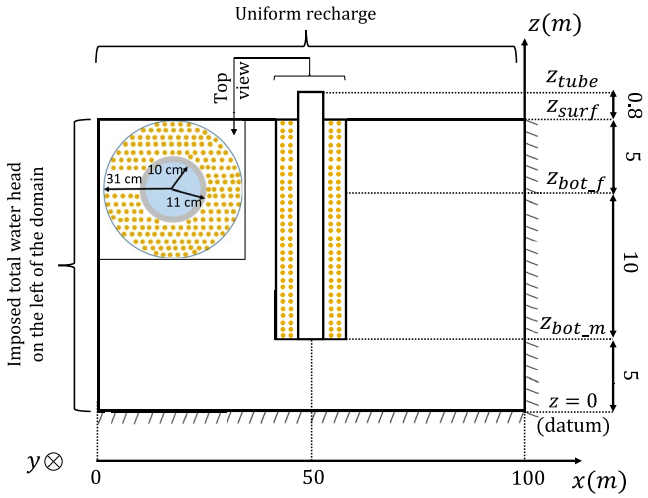

Figure 4. Cross-section at $y = 50$ m of the domain of the synthetic test cases used to assess the suitability ans usefulness of POWeR-FADS. z_{bot_f} is the altitude of lowest interception of the fracture network by the well, and z_{bot_m} is the altitude of the bottom of the well. z_{surf} is the altitude of the surface and z_{tube} is the altitude of the top of the well. The yellow dots represent the material of porosity ω_{drill} used to fill the volume between the tube and the full drilled radius. Total water head at $x = 0$ is imposed at a value that is constant over time, along y and along z. A uniform recharge is applied on the top of the aquifer over the 100*100 m domain. All other sides are impermeable. The well is located at the center of the domain ($x = y = 50$ m).

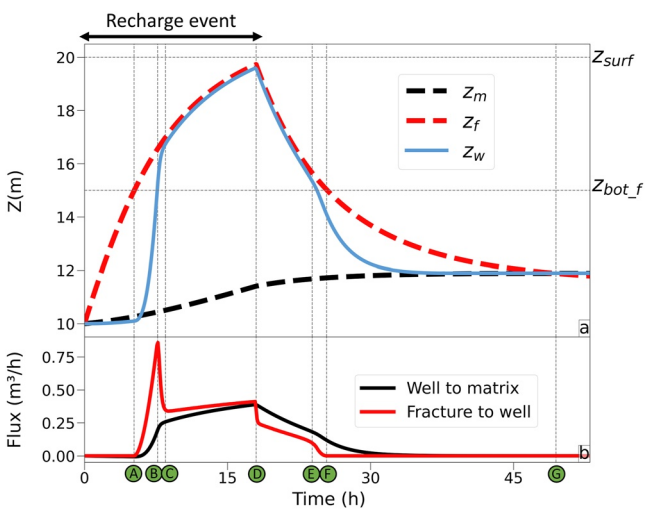

Figure 5. (a): Variation over time of the total water head in the matrix, denoted by z_m, of the total water head in the fracture, denoted by z_f, and of the water level in the observation well, denoted by z_w, for Synthetic Test Case 1. z_m and z_f are simulated by the dual-media hydrogeological model METIS, and z_w is simulated by POWeR-FADS, using z_m and z_f as inputs. z_{bot_f} is the altitude of lowest interception of the fracture network by the well, and z_{surf} is the altitude of the surface. (b) Infiltrated flux from the fracture network into the well and exfiltrated flux from the well into the matrix, as simulated by POWeR-FADS for Synthetic Test Case 1. Times A to G each correspond to particular flow conditions and are commented in the text.

3. Synthetic Test Cases

3.1. Presentation of the Synthetic Test Cases

In order to assess the suitability and usefulness of POWeR-FADS, a set of two synthetic test cases is exposed. They represent a fractured aquifer of dimensions 100*100 m along horizontal directions x and y, and 20 m along the vertical dimension z. A uniform recharge is applied at the top of the aquifer. A total water head that is constant over time, along y and along z, is imposed at $x = 0$. All other sides are impermeable. The domain is monitored by an observation well at its center ($x = y = 50$ m). z_{bot_f} and z_{bot_m} for this well are respectively 5 and 15 m below the surface. Figure 4 provides a cross-section of the domain at $y = 50$ m.

In test 1, the initial conditions, exchange coefficients, and forcing are such that z_m is always below z_{bot_f}, while in test 2, z_m is always above z_{bot_f}. Test 2 displays three consecutive recharge events (5 mm/hr for 5 hr, then 2 mm/hr for 3 hr, and finally 1.1 mm/hr for 3 hr), while test 1 only displays one event (7.2 mm/hr for 18 hr). Moreover, these two tests use different values of porosity and saturated hydraulic conductivity.

z_m and z_f are simulated by the distributed, physically-based hydrogeological model METIS (Goblet, 2017). It implements a finite element method adapting to a bidimensional or tridimensional setting the dual-continuum approach exposed for one-dimensional systems by Gerke and van Genuchten (1993a). In this approach, the exchange fluxes between the fracture medium and the matrix medium are proportional to the difference of water head between the media, following the formulation discussed in Gerke and van Genuchten (1993b). For simulating the synthetic test cases, METIS is set up in a bidimensional approach in the horizontal plane, neglecting all flow in the unsaturated zone. This implies that the infiltration of recharge from the top of the aquifer is not subject to any delay and instantly increases the level of the water table. The meshed domain is a rectangle of dimensions 100*100 m and is composed of 402 triangular elements. The time series for z_m and z_f used as inputs of POWeR-FADS are the values of total water head in the matrix and in the fracture network, respectively, as modeled by METIS at the center of the domain.

Tables A1 and A2 in the appendix list all the parameters to use, in the dual-continuum model and in POWeR-FADS respectively, to replicate the test cases. In both cases, when the well exfiltrates water into the unsaturated zone of a medium, an arithmetic mean is used for calculating $\overline{K}$ (cf. Equation 7).

Figures 5a and 6a display, for Synthetic Test Cases 1 and 2 respectively, the time series for z_m and z_f simulated by METIS, and the time series for z_w modeled nonintrusively from METIS outputs by POWeR-FADS. Figures 5b and 6b display the corresponding exchange fluxes calculated by POWeR-FADS between the well and both media. For both test cases, the POWeR-FADS simulations use less than 0.3 s of CPU time.

3.2. Synthetic Test Case 1: Variations of z_f Above and Below z_{bot_f}, With z_m Always Below z_{bot_f}

At time $t = 0$, the recharge event starts, while the values of z_f, z_m, and z_w are all equal to each other, at a level below z_{bot_f}. As the porosity ω_f in the fracture is about one order of magnitude lower than its matrix counterpart ω_m, z_f increases significantly more quickly than z_m. However, until time A, z_w is not

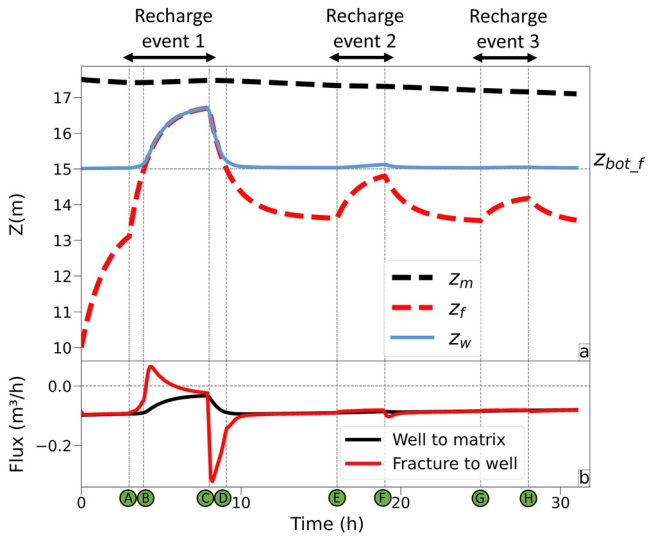

Figure 6. (a): Variation over time of the total water head in the matrix, denoted by z_m, of the total water head in the fracture, denoted by z_f, and of the water level in the observation well, denoted by z_w, for Synthetic Test Case 2. z_m and z_f are simulated by the dual-media hydrogeological model METIS, and z_w is simulated by POWeR-FADS, using z_m and z_f as inputs. z_{bot_f} is the altitude of lowest interception of the fracture network by the well. (b) Infiltrated flux from the fracture network into the well and exfiltrated flux from the well into the matrix, as simulated by POWeR-FADS for Synthetic Test Case 2. Times A to H each correspond to particular flow conditions and are commented in the text.

influenced at all by these variations of z_f. It rather increases slowly, under the influence of z_m. In fact, despite the rise of z_f, the exchange flux between the fracture and the well is null. This is because, during this entire initial rise of z_f, z_w and z_f are such that the integral interval in Equation 6 for $i = f$ is of amplitude zero. This represents the inability of the fracture network to directly exchange water with the well below the level of lower interception of the fractures by the well. In this timeframe, the exchange flux between the matrix and the well is very low, but not null, although it is almost imperceptible in Figure 5b (the flux is actually slightly negative, which means water is going from the matrix to the well). This low exchange rate is mainly due to a low Ks_m and to z_m varying slowly while being initially equal to z_w.

At time A, z_f reaches and then exceeds $z_{\text{bot\_}f}$, which leads to a strong increase of the flux from the fracture to the well. Numerically, this is associated with a modification of the range of the integral in Equation 6 for $i = f$, which becomes $[z_{\text{bot\_}f}; zf]$ (setting similar to Figure 2e). Conceptually, this represents water from the fracture medium overflowing to the well. It is worth noting, however, that the filling of the well with water from the fractures is not instantaneous. Between time A and time B, this delay depends on the dimensions of the well (cf. Equations 3 and 4 where the perimeter and equivalent surface of the well appear). This rise of z_w driven by the evolution of z_f is also partly compensated by leakage flux from the well to the matrix (Figure 5b). This leakage flux happens in a setting illustrated in Figures 3e and 3f, in the range $[z_{\text{bot\_}m}; z_w]$.

At time B, z_w reaches and then exceeds $z_{\text{bot\_}f}$. This leads to a strong drop of the flux from the fracture to the well. The root cause of this phenomenon is that for any z such that $z_{\text{bot\_}f} \leq z \leq z_w$, Equation 5 yields $H_w(z) = z_w$, while for any z such that $z_w \leq z \leq z_f$, Equation 5 yields $H_w(z) = z$. This is crucial, since the intensity of exchanges in Equation 7 directly depends on the difference $H_w(z) - z_f$. As a result, for a given value of z_f, the more the fracture network infiltrates water into a portion of the well filled with air (Figure 2e) instead of a portion of the well filled with water (Figure 2f), the greater the overall infiltrated flux into the well becomes. This explains the observed drop in flux from the fractures to the well between times B and C. Studying the limits of this relationship, it can be observed that, as z_w gradually tends toward z_f, q_i in Equation 7 tends toward 0. This is the main factor imposing a limit on the infiltration rate from the fracture medium into the well. In comparison, the main factor that limits the leakage flow from the well to the matrix is that Ks_m is two orders of magnitude lower than Ks_f (as can reasonably be expected in a fractured porous aquifer), while $|q_i|$ directly depends on Ks_i in Equation 7. At time C and until time D, these two antagonistic limitations seem to reach an equilibrium, as z_w almost reaches z_f with a small and almost constant offset. In fact, this offset enables a quasi-equilibrium between infiltration from the fracture into the well and exfiltration from the well into the matrix, with the difference corresponding to storage of water in the well.

At time D, the recession phase begins: z_f starts decreasing. This reverses the quasi-equilibrium discussed above, as illustrated by red and black curves crossing each other in Figure 5b. Consequently, z_w drops because of greater exfiltration to the matrix than infiltration from the fractures. Then, interestingly, an inflexion point occurs at time E, that is, when z_f is only slightly above $z_{\text{bot\_}f}$. This is because the integral interval in Equation 6 for $i = f$, equal to $[z_{\text{bot\_}f}; z_f]$, has an amplitude that gradually approaches zero, while exchanges between the well and the matrix can still rely on a much greater exchange area ($[z_{\text{bot\_}m}; z_w]$). This implies a relatively more quickly decreasing value of V_f, which becomes gradually weaker compared to V_m, despite the fact that $Ks_f \gg Ks_m$. This is represented in Figure 5b by an increasing difference between the black and red curves. This drives z_w in the direction of z_m, that is, downwards, so that z_w gets even closer to $z_{\text{bot\_}f}$, which fuels this phenomenon exponentially until V_m ends up overwhelming V_f: hence the inflexion point.

The inflexion at time E makes the recession curve change from a concave shape to a convex shape, which is uncommon, until z_f eventually drops below $z_{\text{bot\_}f}$ at time F. At that moment, the amplitude of the integral interval in Equation 6 for $i = f$ becomes equal to zero, so that V_f is null: no more exchanges happen between the well and

the fractures. Consequently, z_w is then exclusively controlled by z_m, except that a delay is needed for the remaining excess water in the well to exfiltrate to the matrix.

Because of the higher values of Ks_i and the lower values of ω_i in the fracture medium than in the matrix, the recession is a lot faster for z_f than for z_m. As a result, at time G, z_f drops below z_m. Yet this has no effect on z_w, which continues to stick to z_m. This is because the amplitude of the integral interval in (6) for $i = f$ is still equal to zero.

As a conclusion, in this first synthetic test case where z_f crosses z_{bot_f} back and forth while z_m is always below z_{bot_f}, POWeR-FADS makes it possible to simulate the following phenomena that could not have been taken into account by simply referring to z_f or z_m alone:

- A delayed but sharp rise of z_w at the start of the recharge event, representing water from the fractures overflowing into the well once z_f exceeds z_{bot_f};
- A persisting offset between z_f and z_w, due to exchanges between the well and the matrix;
- An inflexion accelerating the drawdown velocity at the end of the recession phase (when z_f is close to z_{bot_f}).

3.3. Synthetic Test Case 2: Variations of z_f Above and Below z_{bot_f}, With z_m Always Above z_{bot_f}

At initial conditions, $z_f < z_{bot\_f}$, $z_m > z_{bot\_f}$, and $z_w = z_{bot\_f}$. No recharge event is applied until time A. Before this time, the variations of z_m and z_f simulated by METIS are only due to exchanges between the matrix and the fracture network. During this timeframe, z_w, as simulated by POWeR-FADS, remains constant and equal to z_{bot_f}. This is explained by the exchange fluxes between the well and the media. At the first iteration of convergence of the first time step, no exchange between the well and the fracture is calculated by POWeR-FADS because the range of the integral interval in Equation 6 for the fracture medium is null. On the contrary, water does infiltrate from the matrix into the well, because the integral interval in Equation 6 for the matrix is not null, ranging from z_{bot_m} to z_m, in a setting corresponding to Figures 2e and 2f. But as soon as the water infiltrated from the matrix into the well raises the level of z_w slightly above z_{bot_f}, the range of the integral in Equation 6 for $i = f$ is no longer null, but becomes $[z_{bot\_f}; z_w]$, so that exchanges between the well and the fracture medium are enabled. Provided that the resulting V_f compensates for V_m (which is likely because $Ks_f \gg Ks_m$, and it does indeed happen, as represented in Figure 6b by red and black lines overlapping each other), this phenomenon prevents z_w from rising significantly above z_{bot_f}. This is why z_w remains virtually constant until time A. Conceptually, this represents water from the matrix being transferred to the fracture network through the well by overflowing over z_{bot_f}. As a side note, this demonstrates that the implicit scheme adopted in this work is truly necessary; otherwise, numerical oscillations would be generated in the vicinity of z_{bot_f}.

At time A, a recharge is applied to METIS, which accelerates the rise of z_f. Until time B, z_f gets closer and closer to z_w, but still remains below z_{bot_f}. This causes V_f to become gradually smaller as compared to V_m (see Equations 7 and 5). Because of this drop of V_f, and unlike before time A, POWeR-FADS no longer simulates a situation in which water infiltrating from the matrix into the well is totally transferred to the fracture network. This can be observed in Figure 6b as the red curve gets gradually higher than the black one. This results in z_w increasing slightly while z_f is still below z_{bot_f}.

At time B, z_f reaches and then exceeds z_{bot_f}. Similarly to Synthetic Test Case 1, reaching this threshold enables z_f to be the main driver of the variations of z_w. That said, a notable difference in Synthetic Test Case 2 compared to Synthetic Test Case 1 comes from exchanges between the fracture network and the well changing sign during the recharge event. Just after time B, under the effect of a quickly rising z_f, water starts infiltrating from the fractures into the well (i.e., the red curve enters the positive part of the y-axis in Figure 6b). Then, about halfway between times B and C, the direction of exchanges is reversed back to its original direction (i.e., the red curve becomes negative again). This comes from the combined effect of z_f reaching a plateau and water from the matrix infiltrating continuously into the well, thus raising z_w slightly above z_f (although this offset is imperceptible in Figure 5a).

At time C, the recharge in METIS is stopped, which makes z_f drop quickly. This generates an exfiltrated flux from the well into the fractures that is significantly higher than the infiltrated flux from the matrix into the well, which in turn makes z_w drop. Then, at time D, z_f falls below z_{bot_f}. This leads to a similar case to that observed before time A: POWeR-FADS simulates a "floor effect" that prevents z_w from dropping below z_{bot_f}. Just like before time A, the floor effect is associated with overlapping black and red curves in Figure 6b.

Between times E and F, a second recharge event happens. It makes z_f rise to a level slightly lower than z_{bot_f}. As with the situation between time A and time B, this creates conditions where z_w can reach a value slightly higher than z_{bot_f}, because only part of the water infiltrating from the matrix into the well is directly transferred to the fracture network. This situation is worth presenting as it emphasizes that z_f can have an effect on z_w even without reaching z_{bot_f}.

Finally, a third recharge event happens from time G to time H. Although z_f increases by more than half a meter in response to this input, associated variations of z_w and of fluxes between the well and the media are almost imperceptible. This is actually a repetition of the conditions observed before time A: water infiltrating from the matrix into the well is fully transferred to the fracture medium, because z_f is far enough below z_w to ensure that V_f compensates for V_m as soon as z_w gets just a bit above z_{bot_f}. This stresses that under certain conditions, z_w can be almost totally unaffected by a recharge event.

In conclusion, this second test case shows that when z_f crosses z_{bot_f} back and forth while z_m is always above z_{bot_f}, a "floor effect" is observed. This effect prevents z_w from dropping below z_{bot_f}. Under certain conditions, it can completely preclude z_w from responding to a recharge event.

4. Discussion

4.1. Main Limitations of the Model

4.1.1. Lack of Feedback to the Dual-Continuum Hydrogeological Model

As a postprocessing tool for dual-continuum models, POWeR-FADS presents the main limitation of a lack of feedback on z_m and z_f: exchanges of water between medium i and the well as simulated by POWeR-FADS affect the value of z_w but have no effect on the time series of z_i, which are treated as a forcing data set. For this reason, POWeR-FADS does not make it possible to assess the impact of the presence of the well on the dynamics of flow at the scale of the studied site. It only merges z_m and z_f into a simulated water level in the well, which can then be compared to observation data.

In fact, when POWeR-FADS assumes that z_i is unaffected by the exchanges with the well, the underlying hypothesis is that R_{drill} is negligible compared to the dimensions of the studied site. This is because $\lim_{R_{drill}\to 0} Q_i = 0$ in Equation 6.

In Synthetic Test Cases 1 and 2, assuming in POWeR-FADS that z_m and z_f are unaffected by the exchanges with the well leads to neglecting a total volume transiting between the fractures and the matrix through the well of 8.0 and 2.6 m^3 respectively, which corresponds to about 0.6% and 0.8% of the total recharge, respectively. This demonstrates that the flow processes neglected by POWeR-FADS have indeed a negligible impact at the scale of the 100*100 m domain used for the test cases. Nevertheless, there may still be a non-negligible effect locally around the well. In particular, the difference between z_m and z_f can be expected to drop to some extent as a result of the transfers between the two media through the well, which may hinder the validity of the values of z_w simulated by POWeR-FADS.

In spite of these neglected fluxes, POWeR-FADS remains a tool that embeds far more physical processes than does the usual practice of simply assuming that $z_w \approx z_f$. Besides, the drawbacks implied by the lack of feedback from the developed tool are compensated by its versatility, since it can nonintrusively be plugged into any planar, bidimensional dual-continuum hydrogeological model, without requiring the user to delve into the source code of the chosen model.

4.1.2. Hypothesis of Instantaneous Hydrostatic Equilibrium Along z

POWeR-FADS assumes an instantaneous hydrostatic equilibrium in the well along z below z_w, which is fairly reasonable, because movements of water to reach equilibrium in the well happen at high velocities, given that flow is not slowed down by the presence of any rock in the tube of the well.

POWeR-FADS also makes the same assumption in medium i all along z, both in the saturated zone and in the vadose zone. The validity of this hypothesis is especially debatable in the vadose zone, where hydraulic conductivity can potentially be far lower than Ks_i, thereby preventing an instantaneous hydrostatic equilibrium, generating instead slow infiltration fronts.

Yet this might not have a significant impact on the results obtained using POWeR-FADS. First, the vadose zone is only involved in the calculations when all the following conditions are met simultaneously: $z_w > z_i$, $z_{\text{surf}} > z_i$, and $z_w > z_{\text{bot\_}i}$; and only for any z such that $z_w > z > z_i$. This corresponds to Figure 3e. Besides, in this situation, the well exchanging water with the vadose zone is fully saturated from z_i to z_w (see Figure 3), which ensures a good wetting of the vadose zone in the vicinity of the well from z_i to z_w, and thus leads to non-negligible values of unsaturated hydraulic conductivities compared to Ks_i, which makes the hypothesis of an instantaneous hydrostatic equilibrium more valid.

Overall, the materials for which the assumption of an instantaneous hydrostatic equilibrium are the most valid are those with good infiltration potential, that is, high saturated hydraulic conductivities, and low van Genuchten α and n parameters.

4.1.3. Low-Parameterization of the Vertical Heterogeneity of the Connection Between the Well and the Fracture Network

The only parameter required by POWeR-FADS to describe the vertical heterogeneity of the connection between the well and the fracture network is $z_{\text{bot\_}f}$. As stated in Section 2, the underlying assumption is that the well continuously intercepts the fracture network above $z_{\text{bot\_}f}$, and does not intercept it at all below $z_{\text{bot\_}f}$.

Although simplistic, this hypothesis still makes it possible to simulate all the peculiar flow patterns exhibited in Synthetic Test Cases 1 and 2. Conversely, a hypothetical reversed paradigm would use as the only parameter the altitude of highest interception of the fracture network by the well, denoted by $z_{\text{top\_}f}$, assuming a continuous interception of the fracture network by the well below $z_{\text{top\_}f}$ and no interception at all above $z_{\text{top\_}f}$. However, this hypothetical alternative paradigm would not provide interesting results, because except in the trivial case where $z_{\text{top}_f} = z_{\text{bot}_m}$, fluxes from the fracture to the well would always be enabled provided that $z_f > z_{\text{bot\_}m}$. If, additionally, $Ks_m \ll Ks_f$, which can be expected, this would result in a calculated z_w that is mostly driven by z_f, thus exhibiting none of the main peculiar patterns that the actual POWeR-FADS model is able to reproduce, as exemplified in the synthetic test cases. This illustrates the relevance of using $z_{\text{bot\_}f}$ as the only parameter for POWeR-FADS, in comparison to other equally simple alternatives.

Besides, as exemplified further in Section 4.2.2, reducing the vertical heterogeneity to $z_{\text{bot\_}f}$ appears to be suitable for explaining the hydrographs of on-field wells in which one altitude acts a threshold that imposes a particular behavior on the variations of the observed water level in the well.

4.2. Parameterization of the Model

4.2.1. Global Sensitivity Analysis

As shown in Table A2, apart from parameters regarding numerical convergence (Δt and ε), there are 10 parameters in POWeR-FADS that may need to be calibrated: Ks_m, Ks_f, n_m, n_f, α_m, α_f, R_{drill}, ω_{drill}, $z_{\text{bot\_}f}$, and Δe. Among these, however, only Δe must always be inferred through calibration. Ks_m, Ks_f, n_m, n_f, α_m, and α_f may be inherited from the dual-continuum hydrogeological model used to feed POWeR-FADS with the time series of z_m and z_f, if it also involves these parameters. As for R_{drill}, ω_{drill}, and $z_{\text{bot\_}f}$, they may be obtained from available data.

In order to help the user of POWeR-FADS to determine which parameter requires the greatest investment of time in the calibration exercise, a global sensitivity analysis has been conducted for Synthetic Test Cases 1 and 2 (Jeannot et al., 2022b). It was carried out via Sobol's method (2001), as implemented in PESTPP-SEN (White et al., 2020), by using 100,000 uniformly distributed parameter samples in the intervals detailed in Table A2, and unchanged time series of z_m and z_f from one simulation to another. The results of this sensitivity analysis are in particular the first order and total sensitivity indices for each parameter. The first order sensitivity index relates to the contribution of a parameter by its single effect on the total variance of the output, while the total sensitivity index relates to the full contribution of a parameter on the total variance of the output, either by its single effect or by its interaction with other parameters. As shown in Figure 7, POWeR-FADS appears to be mostly sensitive to $z_{\text{bot\_}f}$, and only slightly sensitive to Ks_m. It is slightly sensitive to Ks_f and Δe, but mainly through interaction with other parameters, and in the case of Δe, only for Synthetic Test Case 1. For other parameters, the sensitivity of POWeR-FADS is marginal, on par with its sensitivity to the convergence criterion.

This shows that, in spite of POWeR-FADS needing 10 parameters, default values such as those displayed in Table A2 could be used systematically, except for four parameters that may be worth tuning: $z_{\text{bot\_}f}$, Ks_m, Ks_f,

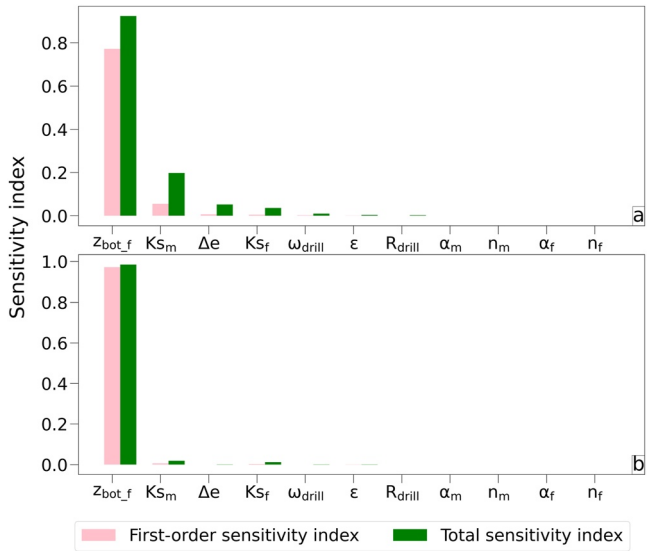

Figure 7. Global sensitivity analysis of POWeR-FADS undertaken using Sobol's method (2001), as implemented in PESTPP-SEN (White et al., 2020), with 100,000 uniformly distributed parameter samples, for (a) Synthetic Test Case 1 and (b) Synthetic Test Case 2. z_{bot_f} is the altitude of lowest interception of the fracture network by the well. Ks_m and Ks_f are the saturated hydraulic conductivities in the matrix and fracture media, respectively. α_m and n_m are van Genuchten coefficients (van Genuchten, 1980) for the matrix, while α_f and n_f are van Genuchten coefficients for the fracture network. Δe is the coupling length, that is, the width of the interface between the well and the media. R_{drill} is the drill radius of the well, and ω_{drill} is the porosity of the material used to fill the space between the tube of the well and R_{drill}. ε is the convergence criterion used by POWeR-FADS. Inputs and outputs of the global sensitivity analysis are archived in Jeannot et al. (2022b).

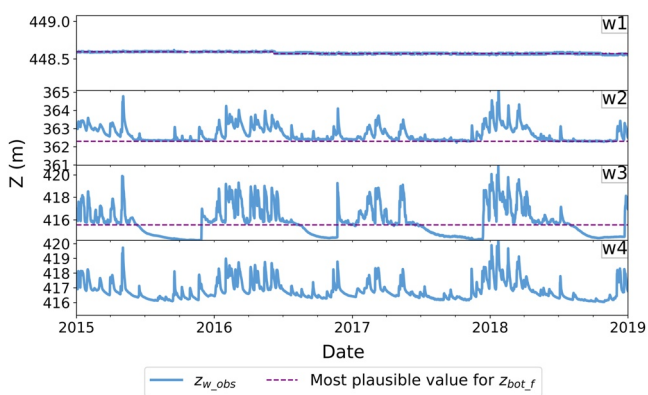

Figure 8. Observed water level, denoted by z_{w_obs}, and most plausible altitude of the last interception of the well by the fracture network, denoted by z_{bot_f}, in four wells from a low-karstified fractured aquifer in Burgundy, France, from 2015 to 2019. For w1, the most plausible value for z_{bot_f} changes after June 2016, possibly because of an actual change in the local geometry of the fractures. For w4, there is no possibility of precisely determining a plausible value of z_{bot_f} from the time series of z_{w_obs}. The time series for z_{w_obs} are archived for the four wells in Commissariat à l'Énergie Atomique et aux Énergies Alternatives (2022).

and Δe. Among these four, Ks_m and Ks_f are likely to be inherited from the dual-continuum hydrogeological model, which would cancel the need for calibrating them. It could also be argued that the sensitivity indices of z_{bot_f} so powerfully overwhelm those of all the other parameters that it may actually be the only parameter worth tuning. This is a crucial point because, in cases where available data make it possible to infer a value of z_{bot_f} on a physical basis without there being a need to tune it, POWeR-FADS could potentially be used without requiring any calibration.

4.2.2. Inferring the Altitude of Lowest Interception of the Fracture Network by the Well on a Physical Basis

In practice, the most straightforward way to infer a suitable value of z_{bot_f} for a given observation well would be to directly search for the lowest observable open fracture in the drill core made in the process of setting up the well. If the drill core is not available, the user of POWeR-FADS might make assumptions about the value of z_{bot_f} by looking at observed time series of the water level in the observation well, denoted by z_{w_obs} [L]. In order to illustrate this, Figure 8 shows time series for four observation wells in a fractured porous aquifer from an observation site in Burgundy, France, between 2015 and 2019. It must be emphasized that the level of karstification of this aquifer is low, with no large karstic conduits (Delbart, 2013). Also, no karstic voids were identified during the drilling of these four wells. Therefore, karstic effects are most likely not the explanation for the patterns observed in the time series.

In Well w1, except for a discontinuity in June 2016 that lowers the average z_{w_obs} by 2 cm from that time onward, z_{w_obs} is almost constant. Without taking into account this discontinuity, the amplitude of variations of z_{w_obs} around the mean is ± 1.5 cm, that is, barely higher than measurement noise. Yet the bottom of the well is much deeper than this almost constant value, and the well is just 60 m away from another one that is not represented and that presents an interval of variations of amplitude 3 m. In POWeR-FADS, this peculiar behavior of w1 could be explained by assuming that z_{bot_f} is equal to the mean value of z_{w_obs}. This way, provided that $Ks_f \gg Ks_m$ and that the simulated values of z_m stay constantly higher than z_{bot_f} while the simulated values of z_f stay sufficiently far below z_{bot_f} (such a difference between z_m and z_f being possible as long as the exchange coefficient between the fractures and the matrix is low enough), POWeR-FADS would succeed in simulating the observed "floor effect," just like between times G and H of Synthetic Test Case 2. As for the discontinuity of June 2016, it could be due to an actual variation of the geometry of the fracture network at the level of lowest interception by the well, possibly because of the high level of recharge in winter and spring 2016 (see the variations of the water level in Wells w2, w3, and w4 over this period). However, at the time of writing of this article, POWeR-FADS does not allow a time-variable value of z_{bot_f}, although this option could be added in the future.

Well w2 presents a floor at $z = 362.3$ m, which can correspond to Synthetic Test Case 2. Indeed, this altitude is often reached but never crossed, yet it does not correspond to the bottom of the well. Reproducing such a time series with alternating sharp recharge events quickly followed by constant base levels (see e.g., April–October 2015) would be difficult and could lead to overfitted parameters if simulated by a dual-continuum hydrogeological model alone. On the contrary, by using POWeR-FADS to postprocess the dual-continuum model and setting z_{bot_f} at $z = 362.3$ m, simulating this alternation of constant and very transient patterns without overfitting parameters

would be more feasible. This would simply require that the simulated values of z_m remain constantly higher than z_{bot_f} and that the simulated values of z_f cross z_{bot_f} back and forth over time.

Well w3 alternatively displays very transient high-flow phases, capped down approximately at $z = 415.55$ m, and inertial phases at low flow displaying almost no response to recharge events. The junction from transient phases to inertial phases is marked by an inflexion, changing the recession curve from a concave to a convex shape. The junction from inertial phases to transient phases is very sharp, always ending up above $z = 415.55$ m, and happens with a delay compared to w2 and w4 (see e.g., the patterns in the last months of years 2017 and 2018, respectively). The authors' interpretation, assuming z_{bot_f} is equal to 415.55 m, is that this well exhibits a pattern similar to Synthetic Test Case 1. This is possible if z_m is below z_{bot_f} at low flows, thus enabling the inflexion point, delayed sharp rise, and total disconnection with the very transient variations of z_f as long as z_f stays below z_{bot_f}, as discussed in Synthetic Test Case 1.

Finally, Well w4 exhibits more classic variations than other wells. Unlike w2, it does not display sharp transitions from very transient states to almost constant phases. Unlike w3, it does not display an inertial pattern smoothing every recharge event at low flows. The authors' interpretation is that w4 is always mostly driven by the variations of z_f. This is possible in POWeR-FADS as long as z_{bot_f} is significantly lower than the minimum of the interval of variations of z_f (see Synthetic Test Case 1 between time C and time E, and Synthetic Test Case 2 between time B and time D).

4.2.3. Method for Averaging Hydraulic Conductivities

An issue in POWeR-FADS comes from the choice given between the geometric and arithmetic mean for calculating $\overline{K}_i$, in the case where water from the well exfiltrates to an unsaturated portion of medium i. In general, the geometric mean is known to better average the hydraulic conductivities at the interface between two heterogeneous blocks than the arithmetic mean, because the latter tends to overestimate the calculated conductivity. (e.g., Belfort & Lehmann, 2005; Haverkamp & Vauclin, 1979). However, in the nonintrusive framework chosen for plugging POWeR-FADS into the dual-continuum hydrogeological model, the progressive wetting of the initially unsaturated medium by water from a well with a high z_w is not directly taken into account, which tends to lead to an underestimation of the calculated hydraulic conductivities. This underestimation might be compensated to some extent by the overestimation that arises when one uses an arithmetic mean to calculate $\overline{K}_i$.

4.3. Particular Cases and Transposability

4.3.1. POWeR-FADS and Confined Aquifers

As stated in Section 1 and as taken into account in the equations of Section 2.2, POWeR-FADS can be applied in the case of confined aquifers. There are only two points to consider compared to the case of unconfined aquifers. First, the water level in the well is capped at z_{tube}, to incorporate the possibility of water overflowing from the top of the tube. Second, although z_w and z_i are both greater than z_{surf}, the exchange surface between the well and the media is capped at the higher end by z_{surf}, as implemented in Equation 6.

Yet for the sake of conciseness, Section 3 does not present a test case in a confined setting. This is because flow processes do not exhibit very peculiar patterns in confined aquifers as compared to unconfined aquifers. Indeed, for confined aquifers, by definition, $z_i \geq z_{surf} \geq z_{bot\_f}$. In this setting, similarly to Synthetic Test Case 1 between times C and E, and Synthetic Test Case 2 between times B and D, z_w is mostly driven by z_f, provided that $Ks_m \ll Ks_f$, with an offset that accounts for exchange between the well and the matrix.

4.3.2. POWeR-FADS and Dual-Porosity Models

Theoretically, POWeR-FADS can be used to postprocess the results of any bidimensional dual-continuum model—either a dual-porosity or dual-permeability model—as long as it provides time series for z_m and z_f. That said, POWeR-FADS also requires information on the properties of both media (Table A2). This becomes a problem for dual-porosity models as they intrinsically assume that $Ks_m = 0$. In the dual-continuum model, such an assumption is relevant, because generally $Ks_m \ll Ks_f$. Nevertheless, in POWeR-FADS, Ks_f may have strictly no influence on the exchanges of water with the well, so that the exchange term involving Ks_m is the one driving the variations of z_w (e.g., Synthetic Test Case 1 before time A). For this reason, even when using a dual-porosity model as input, a nonzero value of Ks_m should be set in POWeR-FADS.

4.3.3. POWeR-FADS and Piezometers

The observation wells discussed in this article are designed to interact with the aquifer along the entire water column through their perforated tubing. This makes it possible to measure an averaged water head over the vertical direction. On the contrary, piezometers (also called cased wells) are designed to measure water head only for a given layer. This is done by encasing the well with an impermeable material on the whole column, except around the altitude of interest, where a screen allows water exchanges with the media.

Theoretically, replacing z_{surf} by the altitude of the top of the screen and $z_{\text{bot\_}f}$ by the altitude of lowest interception of the fracture network by the screen in the governing equations of POWeR-FADS would be enough to adapt the model to piezometers. However, using POWeR-FADS in such cases may only rarely be useful, as detailed below.

First of all, since the screen covers only a small part of the aquifer, there is a reasonable possibility that the screen will intercept no fracture at all. In that case, using POWeR-FADS to simulate z_w would provide similar results to simply assuming that $z_w = z_m$, with the exception of a possible delay effect if Ks_m is extremely low.

If, on the contrary, the aquifer is fractured enough to ensure that the screen does intercept the fracture network, the relevance of using POWeR-FADS depends on the altitude of the screen. In the case where the screen is located below the interval of variations of z_f, this would also imply $z_f > z_{\text{bot\_}f}$. Under these circumstances, provided that $Ks_m \ll Ks_f$, Synthetic Test Case 1 between times C and E, and Synthetic Test Case 2 between times B and D show that using POWeR-FADS to simulate z_w would provide results very similar to what would be obtained by simply assuming that $z_w = z_f$.

As a result, generally, using POWeR-FADS for a piezometer is relevant only if the screen intercepts the fracture network, and if it is not located below the lower limit of the interval of variations of z_f.

4.3.4. POWeR-FADS and Pumping Wells

Pumping wells generate nonhorizontal flow around them: this results in a drawdown cone. This contradicts the hypothesis of an instantaneous hydrostatic equilibrium along z used by POWeR-FADS, because this hypothesis implies that total water head is constant along z (see Figures 2a and 3a), which is not compatible with the presence of a drawdown cone. This hinders the ability of POWeR-FADS to model pumping wells accurately.

Another issue when dealing with pumping wells in POWeR-FADS comes from the lack of feedback on z_f and z_m discussed previously. During a pumping test, the pumped flow depletes water from the well, which in turn generates a significant decrease of z_f and z_m in the vicinity of the well. However, since POWeR-FADS does not provide feedback on z_f and z_m, this flow process cannot be simulated directly in the developed tool. The alternative is to apply the pumped flow as a sink term directly in the dual-continuum model used as an input of POWeR-FADS. Nevertheless, doing so would require that the sink term be arbitrarily split between the matrix and the fractures, which does not allow an optimal description of flow processes. The solution to this issue would be to undertake a two-way coupling, with a feedback on z_f and z_m, between the physics embedded in POWeR-FADS and a dual-continuum hydrogeological model. Nevertheless, this is outside the scope of the present study.

For these reasons, the authors advise against applying POWeR-FADS to pumping wells.

5. Conclusions

Dual-continuum models of fractured porous aquifers can produce as output, at the location of observation wells, the time series of total water head in the matrix medium and in the fracture network, denoted respectively by z_m and z_f. By postprocessing these outputs, POWeR-FADS (archived in Jeannot et al. (2022a) and available at https://github.com/BJeannot1/POWeR-FADS) enables its user to reproduce various peculiar variations of water level in observation wells, denoted by z_w, over time. The authors explain most of these variation patterns as the consequence of a fracture network that is no longer intercepted by the well below a certain altitude denoted by $z_{\text{bot\_}f}$ (see Figure 1). The aforementioned patterns include the following, as illustrated in Synthetic Test Cases 1 and 2 (Figures 5 and 6):

- A floor effect when $z_m > z_{\text{bot\_}f} > z_f$, which prevents z_w from dropping below $z_{\text{bot\_}f}$. This is due to water from the matrix being transferred to the fracture network through the well by overflowing above the altitude of the lowest interception of the fracture network by the well;

- A delayed but sharp rise in z_w at the start of a recharge event when $z_m \leq z_{\text{bot\_}f}$, representing water from the fractures overflowing into the well once z_f exceeds $z_{\text{bot\_}f}$;
- An inflexion accelerating the drawdown velocity during the recession phase, when z_f approaches $z_{\text{bot\_}f}$ while $z_m \leq z_{\text{bot\_}f}$;
- A persisting offset that prevents z_w from exactly reaching z_f, and that represents exchanges between the well and the matrix.

The main drawback of POWeR-FADS comes from its lack of feedback on the dual-continuum model: calculated exchange fluxes between the well and the media are assumed to affect only z_w, and neither z_m nor z_f. However, the positive aspect of such an assumption is the nonintrusive nature of POWeR-FADS, which enables this tool to be plugged into any bidimensional dual-continuum hydrogeological model without requiring the user to delve into its source code. This will provide modelers with a readily available physics-based alternative to the common practice of simply assuming that $z_w \approx z_f$. Another aspect that makes POWeR-FADS handy is its low need for calibration: it is mainly sensitive to $z_{\text{bot\_}f}$, which might be deduced either from drill cores or from analyzing the time series of observed z_w.

There are several ways in which POWeR-FADS could possibly be improved in the future. First, in order to easily deal with the case where drill cores are not available to provide information about the value of $z_{\text{bot\_}f}$, an algorithm could be created to use time series of observed z_w to automatically determine the most plausible value of $z_{\text{bot\_}f}$ (this has been done manually in the discussion for the four wells whose time series are presented in Figure 8).

Second, a more complex profile pressure than the hydrostatic one used in the present study could be chosen in order to better take into account the unsaturated zone.

Third, a calculation of the temperature and of the concentration of dissolved species in the observation well, computed nonintrusively as a function of the previously modeled values for the matrix medium and for the fracture network, could be added to the tool. Such a development would improve the interpretation of temperature and concentration field data in fractured aquifers.

Finally, the vertical description of the connections between the fracture network and the well could be complexified compared to the current parameterization, which only requires the value of $z_{\text{bot\_}f}$. This could be useful in particular for simulating observation wells whose drill cores are available for providing detailed data on the interceptions of the fracture network by the well.

Notwithstanding these future improvements to be made, the authors expect that users of dual-continuum models will benefit from POWeR-FADS, since by postprocessing their results with this program, they will manage to fit their models to reproduce observation data sets with a reduced risk of overfitting hydrodynamic parameters such as porosity, saturated hydraulic conductivity, specific storage coefficients, or van Genuchten coefficients. To demonstrate this, a further study will undertake an inverse problem of a bidimensional dual-continuum model of a real fractured aquifer, both with and without postprocessing the results of the model with POWeR-FADS, and will then assess to what extent the use of POWeR-FADS leads to optimized forecast bias and uncertainties, compared to not using this tool.

Appendix A: Parameters for Synthetic Test Cases 1 and 2

Tables A1 and A2 detail all the parameters used respectively by METIS (Goblet, 2017) and POWeR-FADS for simulating Synthetic Test Cases 1 and 2.

Table A1
Parameters Used by METIS (Goblet, 2017) for Synthetic Test Cases 1 and 2

Parameter name	Short name	Unit	Test 1	Test 2
Boundary conditions				
Uniform Initial Total Water Head in the Matrix	z_{m0}	m	10	17.5
Uniform Initial Total Water Head in the Fractures	z_{f0}	m	10	
Imposed Total Water Head at $x = 0$ for the Matrix	z_{m_left}	m	10	

Table A1
Continued

Parameter name	Short name	Unit	Test 1	Test 2
Imposed Total Water Head at $x = 0$ for the Fractures	z_{f_left}	m	10	
Recharge events				
Start and End Time of the First Recharge Event	$[ts_1; tf_1]$	h	[0;18]	[3;8]
Recharge Intensity for the Fracture (First Event)	I_{f1}	$m.s^{-1}$	1.5E−06	9.0E−07
Recharge Intensity for the Matrix (First Event)	I_{m1}	$m.s^{-1}$	5.0E−07	5.0E−07
Start and End Time of the Second Recharge Event	$[ts_2; tf_2]$	h	-	[16;19]
Recharge Intensity for the Fracture (Second Event)	I_{f2}	$m.s^{-1}$	-	3.7E−07
Recharge Intensity for the Matrix (Second Event)	I_{m2}	$m.s^{-1}$	-	2.0E−07
Start and End Time of the Third Recharge Event	$[ts_3; tf_3]$	h	-	[25;28]
Recharge Intensity for the Fracture (Third Event)	I_{f3}	$m.s^{-1}$	-	2.0E−07
Recharge Intensity for the Matrix (Third Event)	I_{m3}	$m.s^{-1}$	-	1.0E−07
Hydrodynamic parameters of the matrix medium				
Porosity of the Matrix	ω_m	-	0.08	0.12
Saturated Hydraulic Conductivity of the Matrix	Ks_m	$m.s^{-1}$	1.0E−07	5.0E−08
Specific Storage Coefficient of the Matrix	Ss_m	m^{-1}	1.0E−08	
Hydrodynamic parameters of the fracture medium				
Porosity of the Fracture Network	ω_f	-	0.007	0.002
Saturated Hydraulic Conductivity of the Fracture Network	Ks_f	$m.s^{-1}$	1.0E−05	6.0E−05
Specific Storage Coefficient of the Fracture Network	Ss_f	m^{-1}	1.0E−08	
Parameters defining the exchange flux between the fractures and the matrix				
Coefficient β Gerke and van Genuchten (1993b)	β	-	3.0	
Coefficient a Gerke and van Genuchten (1993b)	a	m	1.0	
Coefficient γ_ω Gerke and van Genuchten (1993b)	γ_ω	-	0.4	
Saturated Hydraulic Conductivity at the Interface between Fracture and Matrix	Ks_{int}	$m.s^{-1}$	1.0E−08	
Parameters regarding numerical convergence				
Time Step	Δt	s	360	
Convergence Criterion	ε	m	1.0E−5	

Table A2
Parameters Used by POWeR-FADS for Synthetic Test Cases 1 and 2

Parameter name	Short name	Unit	Value for test 1	Value for test 2	Range for the sensitivity analysis
Parameters that are directly measurable on-field					
Altitude of the Top of the Tube of the Well	z_{tube}	m	20.8		/
Altitude of the Surface	z_{surf}	m	20		/
Altitude of the Bottom of the Well	z_{bot_m}	m	5		/
Inner Radius of the Observation Well	R_{in}	m	0.10		/
Outer Radius of the Observation Well	R_{out}	m	0.11		/
Initial Water Level in the Observation Well	$z_{\omega 0}$	m	10	15	/
Parameters that may be either calibrated or, when applicable, inherited from the dual-continuum hydrological model					
Saturated Hydraulic Conductivity of the Matrix	Ks_m	$m.s^{-1}$	1.0E−7	5.0E−8	[1.0E−9; 1.0E−6]
Saturated Hydraulic Conductivity of the Fracture Network	Ks_f	$m.s^{-1}$	1.0E−5	6.0E−5	[5.0E−6; 5.0E−3]

Table A2
Continued

Parameter name	Short name	Unit	Value for test 1	Value for test 2	Range for the sensitivity analysis
Coefficient n for the Matrix van Genuchten (1980)	n_m	-	2		[1.2; 2.5]
Coefficient α for the Matrix van Genuchten (1980)	α_m	m^{-1}	2		[0.5; 4]
Coefficient n for the Fracture Network van Genuchten (1980)	n_f	-	2		[1.2; 2.5]
Coefficient α for the Fracture Network van Genuchten (1980)	α_f	m^{-1}	10		[2; 20]
Parameters that may be either calibrated or obtained from available data					
Drill Radius of the Observation Well	R_{drill}	m	0.31		[0.21; 0.41]
Porosity of the Material Used to Fill the Space between the Tube of the Well and the Drill Radius	ω_{drill}	-	0.4		[0.1; 0.45]
Altitude of Lowest Interception of the Fracture Network by the Well	z_{bot_f}	m	15		[5; 20]
Parameter that can only be inferred through calibration					
Coupling Length between the Well and the Media	Δe	m	0.1		[0.01;0.2]
Parameters regarding numerical convergence					
Convergence Criterion	ϵ	m	1.0E−5		[1.0E−6; 1.0E−2]
Time Step	Δt	s	360		/

Data Availability Statement

The source code of POWeR-FADS, along with the inputs needed for running it for Synthetic Test Cases 1 and 2, are archived in Jeannot et al. (2022a) and available in their latest release on GitHub at https://github.com/BJeannot1/POWeR-FADS. PESTPP-SEN, in its version 5.1.24, which was used for performing the global sensitivity analysis, is available in the supplementary materials of White et al. (2020). The inputs and outputs of the global sensitivity analysis performed are archived in Jeannot et al. (2022b). The on-field observation data set used in Figure 8 is archived in Commissariat à l'Énergie Atomique et aux Énergies Alternatives (2022). The METIS dual-continuum hydrogeological model is not openly distributed but may be obtained on request; the contact details of its developer and a presentation of the program are available at https://www.geosciences.minesparis.psl.eu/systemes-hydrologiques-et-reservoirs/metis-cimlib/.

Acknowledgments
This work was supported by the LRC Yves Rocard (Laboratoire de Recherche Conventionné CEA-ENS-CNRS) under the project titled "Modélisation hydrogéologique d'un aquifère calcaire fissuré: double porosité et transport," and the global sensitivity analysis was run on the "Centre de Calcul Recherche et Technologie" computing cluster of the Commissariat à l'Énergie Atomique et aux Énergies Alternatives. Finally, the authors would like to thank François Renard for his valuable suggestions.

References

Ackerer, P., Trottier, N., & Delay, F. (2014). Flow in double-porosity aquifers: Parameter estimation using an adaptive multiscale method. *Advances in Water Resources*, *73*, 108–122. https://doi.org/10.1016/j.advwatres.2014.07.001

Al-Shaalan, T., Fung, L., & Dogru, A. (2003). *A scalable massively parallel dual-porosity dual-permeability simulator for fractured reservoirs with super-K permeability*. Paper presented at the SPE Annual Technical Conference and Exhibition. https://doi.org/10.2118/84371-MS

Barenblatt, G., Zheltov, I., & Kochina, I. (1960). Basic concepts in the theory of seepage of homogeneous liquids in fissured rocks. *Journal of Applied Mathematics and Mechanics*, *24*(5), 1286–1303. https://doi.org/10.1016/0021-8928(60)90107-6

Belfort, B., & Lehmann, F. (2005). Comparison of equivalent conductivities for numerical simulation of one-dimensional unsaturated flow. *Vadose Zone Journal*, *4*(4), 1191–1200. https://doi.org/10.2136/vzj2005.0007

Berkowitz, B. (2002). Characterizing flow and transport in fractured geological media: A review. *Advances in Water Resources*, *25*(8–12), 861–884. https://doi.org/10.1016/S0309-1708(02)00042-8

Berre, I., Doster, F., & Keilegavlen, E. (2019). Flow in fractured porous media: A review of conceptual models and discretization approaches. *Transport in Porous Media*, *130*(1), 215–236. https://doi.org/10.1007/s11242-018-1171-6

Bogdanov, I., Mourzenko, V., Thovert, J., & Adler, P. (2003). Pressure drawdown well tests in fractured porous media. *Water Resources Research*, *39*(1), 289–310. https://doi.org/10.1029/2000WR000080

Choi, E., Cheema, T., & Islam, M. (1997). A new dual-porosity/dual-permeability model with non-Darcian flow through fractures. *Journal of Petroleum Science and Engineering*, *17*(3–4), 331–344. https://doi.org/10.1016/S0920-4105(96)00050-2

Commissariat à l'Énergie Atomique et aux Énergies Alternatives. (2022). Observed water level from 2015 to 2019 in 4 wells from a porous fractured aquifer in Burgundy, France [Dataset]. Zenodo. https://doi.org/10.5281/zenodo.7248286

Delay, F., Ackerer, P., & Guadagnini, A. (2011). Theoretical analysis and field evidence of reciprocity gaps during interference pumping tests. *Advances in Water Resources*, *34*(5), 592–606. https://doi.org/10.1016/j.advwatres.2011.02.006

Delay, F., Badri, H., Fahs, M., & Ackerer, P. (2017). A comparison of discrete versus continuous adjoint states to invert groundwater flow in heterogeneous dual porosity systems. *Advances in Water Resources*, *110*, 1–18. https://doi.org/10.1016/j.advwatres.2017.09.022

Delbart, C. (2013). *Variabilité spatio-temporelle du fonctionnement d'un aquifère karstique du Dogger: suivis hydrodynamiques et géochimiques multifréquences; traitement du signal des réponses physiques et géochimiques (Doctoral dissertation)*. Université Paris Sud. Retrieved from https://www.theses.fr/2013PA112290

Dougherty, D., & Babu, D. (1984). Flow to a partially penetrating well in a double-porosity reservoir. *Water Resources Research*, *20*(8), 1116–1122. https://doi.org/10.1029/WR020i008p01116

Flemisch, B., Berre, I., Boon, W., Fumagalli, A., Schwenck, N., Scotti, A., et al. (2018). Benchmarks for single-phase flow in fractured porous media. *Advances in Water Resources*, *111*, 239–258. https://doi.org/10.1016/j.advwatres.2017.10.036

Gerke, H., & van Genuchten, M. (1993a). A dual-porosity model for simulating the preferential movement of water and solutes in structured porous media. *Water Resources Research*, *29*(2), 305–319. https://doi.org/10.1029/92WR02339

Gerke, H., & van Genuchten, M. (1993b). Evaluation of a first-order water transfer term for variably saturated dual-porosity flow models. *Water Resources Research*, *29*(4), 1225–1238. https://doi.org/10.1029/92WR02467

Goblet, P. (2017). *Programme METIS: Simulation d'écoulement et de Transport Miscible en Milieu Poreux et Fracturé—Notice de conception—Mise à jour au 31/08/2017*. Geosciences Departmant Technical Report.

Haverkamp, R., & Vauclin, M. (1979). A note on estimating finite difference interblock hydraulic conductivity values for transient unsaturated flow problems. *Water Resources Research*, *15*(1), 181–187. https://doi.org/10.1029/WR015i001p00181

Hu, R., & Walsh, S. (2021). Effective continuum approximations for permeability in brown-coal and other large-scale fractured media. *Geosciences*, *11*(12), 511. https://doi.org/10.3390/geosciences11120511

Hyman, J., Sweeney, M., Gable, C., Svyatsky, D., Lipnikov, K., & David Moulton, J. (2022). Flow and transport in three-dimensional discrete fracture matrix models using mimetic finite difference on a conforming multi-dimensional mesh. *Journal of Computational Physics*, *466*, 111396. https://doi.org/10.1016/j.jcp.2022.111396

Jazayeri Noushabadi, M., Jourde, H., & Massonnat, G. (2011). Influence of the observation scale on permeability estimation at local and regional scales through well tests in a fractured and karstic aquifer (Lez aquifer, Southern France). *Journal of Hydrology*, *403*(3–4), 321–336. https://doi.org/10.1016/j.jhydrol.2011.04.013

Jeannot, B., Schaper, L., & Habets, F. (2022a). Program for observation well representation in fractured aquifer dual-continuum simulations (version 1.3) [Software]. Zenodo. https://doi.org/10.5281/zenodo.7248614

Jeannot, B., Schaper, L., & Habets, F. (2022b). Global sensitivity analysis for the program for observation well representation in fractured aquifer dual-continuum simulations (version 1.2) [Dataset]. Zenodo. https://doi.org/10.5281/zenodo.7248798

Kaczmaryk, A., & Delay, F. (2007a). Improving dual-porosity-medium approaches to account for karstic flow in a fractured limestone: Application to the automatic inversion of hydraulic interference tests (Hydrogeological Experimental Site, HES—Poitiers—France). *Journal of Hydrology*, *347*(3–4), 391–403. https://doi.org/10.1016/j.jhydrol.2007.09.027

Kaczmaryk, A., & Delay, F. (2007b). Interference pumping tests in a fractured limestone (Poitiers—France): Inversion of data by means of dual-medium approaches. *Journal of Hydrology*, *337*(1–2), 133–146. https://doi.org/10.1016/j.jhydrol.2007.01.025

Liu, E., Hudson, J., & Pointer, T. (2000). Equivalent medium representation of fractured rock. *Journal of Geophysical Research*, *105*(B2), 2981–3000. https://doi.org/10.1029/1999JB900306

Lorentz, H. A. (1896). The theorem of Poynting concerning the energy in the electromagnetic field and two general propositions concerning the propagation of light. *Amsterdammer Akademie der Wetenschappen*, *4*, 176.

MousaviMirkalaei, S. M., Primasari, I., Purwatiningsih, N., Edmondson, M., & Wicakson, A. (2022). A new reservoir simulation approach for modelling of naturally fractured reservoir in an onshore Indonesian mature field. In *Paper presented at the offshore technology conference Asia*. Kuala Lumpur. https://doi.org/10.4043/31389-MS

Mualem, Y. (1976). A new model for predicting the hydraulic conductivity of unsaturated porous media. *Water Resources Research*, *12*(3), 513–522. https://doi.org/10.1029/WR012i003p00513

Neuman, S. (2005). Trends, prospects and challenges in quantifying flow and transport through fractured rocks. *Hydrogeology Journal*, *13*(1), 124–147. https://doi.org/10.1007/s10040-004-0397-2

Peters, R., & Klavetter, E. (1988). A continuum model for water movement in an unsaturated fractured rock mass. *Water Resources Research*, *24*(3), 416–430. https://doi.org/10.1029/WR024i003p00416

Robineau, T., Tognelli, A., Goblet, P., Renard, F., & Schaper, L. (2018). A double medium approach to simulate groundwater level variations in a fissured karst aquifer. *Journal of Hydrology*, *565*, 861–875. https://doi.org/10.1016/j.jhydrol.2018.09.002

Rüdiger, F., Dentz, M., Nimmo, J., & Kordilla, J. (2022). Laboratory experiments and dual-domain modeling of infiltration dynamics in partially saturated fractured porous media. *Vadose Zone Journal*, *21*(2). https://doi.org/10.1002/vzj2.20177

Saevik, P., Jakobsen, M., Lien, M., & Berre, I. (2014). Anisotropic effective conductivity in fractured rocks by explicit effective medium methods. *Geophysical Prospecting*, *62*(6), 1297–1314. https://doi.org/10.1111/1365-2478.12173

Sanchez-Vila, X., Ackerer, P., Delay, F., & Guadagnini, A. (2016). Characterization of reciprocity gaps from interference tests in fractured media through a dual porosity model. *Water Resources Research*, *52*(3), 1696–1704. https://doi.org/10.1002/2015wr018171

Sandve, T., Berre, I., & Nordbotten, J. (2012). An efficient multi-point flux approximation method for Discrete Fracture–Matrix simulations. *Journal of Computational Physics*, *231*(9), 3784–3800. https://doi.org/10.1016/j.jcp.2012.01.023

Sobol, I. (2001). Global sensitivity indices for nonlinear mathematical models and their Monte Carlo estimates. *Mathematics and Computers in Simulation*, *55*(1–3), 271–280. https://doi.org/10.1016/s0378-4754(00)00270-6

van Genuchten, M. T. (1980). A closed-form equation for predicting the hydraulic conductivity of unsaturated soils. *Soil Science Society of America Journal*, *44*(5), 892–898. https://doi.org/10.2136/sssaj1980.03615995004400050002x

Wang, L., Xiang, Y., Hu, J., Li, T., Cai, C., & Cai, J. (2020). Unsteady flow to a partially penetrating pumping well with wellbore storage in a dual-permeability confined aquifer. *Journal of Hydrology*, *591*, 125345. https://doi.org/10.1016/j.jhydrol.2020.125345

Warren, J., & Root, P. (1963). The behavior of naturally fractured reservoirs. *Society of Petroleum Engineers Journal*, *3*(03), 245–255. https://doi.org/10.2118/426-PA

White, J. T., Hunt, R. J., Doherty, J. E., & Fienen, M. N. (2020). Approaches to highly parameterized inversion: Pest++ version 5, a software suite for parameter estimation, uncertainty analysis, management optimization and sensitivity analysis. *US Geological Survey Techniques and Methods*, *7C26*, 51. https://doi.org/10.3133/tm7C26